Nonlinear Backstepping Control of SynRM Drive Systems Using Reformed Recurrent Hermite Polynomial Neural Networks with Adaptive Law and Error Estimated Law

Jung-Chu Ting[†] and Der-Fa Chen[*]

[†,*]Dept. of Industrial Education and Technology, National Changhua University of Education, Changhua, Taiwan

Abstract

The synchronous reluctance motor (SynRM) servo-drive system has highly nonlinear uncertainties owing to a convex construction effect. It is difficult for the linear control method to achieve good performance for the SynRM drive system. The nonlinear backstepping control system using upper bound with switching function is proposed to inhibit uncertainty action for controlling the SynRM drive system. However, this method uses a large upper bound with a switching function, which results in a large chattering. In order to reduce this chattering, a nonlinear backstepping control system using an adaptive law is proposed to estimate the lumped uncertainty. Since this method uses an adaptive law, it cannot achiever satisfactory performance. Therefore, a nonlinear backstepping control system using a reformed recurrent Hermite polynomial neural network with an adaptive law and an error estimated law is proposed to estimate the lumped uncertainty and to compensate the estimated error in order to enhance the robustness of the SynRM drive system. Further, the reformed recurrent Hermite polynomial neural network with two learning rates is derived according to an increment type Lyapunov function to speed-up the parameter convergence. Finally, some experimental results and a comparative analysis are presented to verify that the proposed control system has better control performance for controlling SynRM drive systems.

Key words: Backstepping control, Recurrent Hermite polynomial neural network, Synchronous reluctance motor

I. INTRODUCTION

The synchronous reluctance motor (SynRM) has long been regarded as inferior to other type of AC motors. The SynRM has been mainly used for variable-frequency applications in pumps and fiber spinning machines [1], [2]. However, the SynRM has many advantages. When compared to the direct current motor (DCM), there are no slip rings or commutators [2]. When compared to the permanent magnet synchronous motor (PMSM), there are no permanent magnets [2]. When compared to other servomotors, the SynRMs have a higher efficiency and a lower cost through optimal design methods

[3]-[5]. Owing to advances in motor design and power electronics, many researchers have conducted research on the drive and control of SynRMs [6]-[10]. Lipo et al. [6] studied the vector control of a SynRM including saturation and core loss. Betz et al. [7] introduced four kinds of torque control methods for SynRMs. Lin [8] proposed an adaptive recurrent fuzzy neural network control system t controlling SynRM servo drives. Wei et al. [9] evolved an online tuning adaptive controller design for SynRM drive systems according to the least-mean-square algorithm. Chiang et al. [10] developed a reference adaptive Hermite fuzzy neural network controller for the SynRM to estimate the lumped uncertainty of the system. However, these adaptive control methods were proposed for controlling SynRM drive systems to the improve control performance.

The recursive backstepping design methodology was originally introduced in adaptive control theory to systematically

construct the feedback control law, the parameter adaptation law and the associated Lyapunov function for a class of nonlinear systems satisfying certain structured properties. The idea of a backstepping design is to recursively select some appropriate functions of state variables as pseudo-control inputs for lower dimension subsystems of the overall system. Each backstepping stage results in a new pseudo-control design, which is expressed in terms of the pseudo control designs from the preceding design stages. When the procedure terminates, a feedback design for the true control input results, which achieves the original design objective by virtue of a final Lyapunov function formed by summing up the Lyapunov functions associated with each of the individual design stages [11], [12]. Some of these methods use off-line data collected from the machine during static conditions, which change during motor operation due to changes in the motor parameters. Some methods use a linear model of the machine, which may not be suitable for high-performance applications under the occurrence of uncertainties.

In recent years, intelligent control including fuzzy logic control and neural network control has been widely applied to drive motors [13]-[16]. Amer et al. [13] presented a comparison of different intelligent control techniques for a PM dc motor. Lin [14] proposed backstepping control of LSM drive systems using an adaptive modified recurrent Laguerre OPNNUO. Payam et al. [15] developed a robust DTC control of doubly-fed induction machines based on input-output feedback linearization using recurrent neural networks. Lin [16] proposed hybrid recurrent wavelet neural network control of a PMSM servo-drive system for electric scooters. Due to their good learning, neural networks [14]-[16] with a parallel structure possess a better ability to approximate the modeling of nonlinear systems. However, they are computationally expensive and yield a large number of iterations for training. To reduce the computational complexity, a functional-type neural network [17]-[19] with a lot less computational cost has been introduced. It is shown that the performance of the functional-link neural network is similar to that of a neural network but with a faster convergence and less computational complexity. Additionally, Ma et al. [20], [21] proposed a computationally efficient Hermite polynomial neural network. Constructing Hermite polynomial expansions were adopted by using structure and function levels adaptation methodologies. This Hermite polynomial neural network can effectively map the underlying input-output map. Rigatos et al. [22] proposed a Hermite polynomial neural network that can be used in the nonparametric estimation. Siniscalchi et al. [23] proposed a Hermite polynomial neural network for application in connectionist speech recognition systems with speaker adaptation. However, these Hermite polynomial neural networks have also been applied for system modelling and image processing. Moreover, the weight updates of these neural networks utilizes the internal

information of the neural networks and senses the function approximation in the training procedure. Due to greater precision approximations in modeling nonlinear systems and dynamic control [17]-[19], many researchers have been fascinated with recurrent neural network studies. These recurrent neural networks are able to carry out the identification and control of complex dynamics system. However, they also have higher computational costs. The proposed reformed recurrent Hermite polynomial neural network has better dynamic mapping performance and less computational time in the presence of uncertainties. This paper presents a nonlinear backstepping control system using a reformed recurrent Hermite polynomial neural network with an adaptive law and an error estimated law for controlling SynRM drive systems to enhance robustness.

This paper is organized as follows. The system structure of the SynRM drive system is reviewed in Section II. The design method of a nonlinear backstepping control system is presented in Section III. Experimental results and comparative studies for various control methods are illustrated in Section IV. Some conclusions are given in Section V.

II. CONFIGURATION OF A SynRM DRIVE SYSTEM

The machine model of a SynRM in the synchronously rotating reference frame can be offered in the following descriptions [6]-[8]:

$$u_Q = r_s\, i_Q + \dot{\lambda}_Q + \omega_s \lambda_D \qquad (1)$$

$$u_D = r_s\, i_D + \dot{\lambda}_D - \omega_s \lambda_Q \qquad (2)$$

and:

$$\lambda_Q = L_Q\, i_Q \qquad (3)$$

$$\lambda_D = L_D\, i_D \qquad (4)$$

$$\omega_s = P\,\omega_r\, /\, 2 \qquad (5)$$

where u_D and u_Q are the D axis and Q axis stator voltages, i_D and i_Q are the D axis and Q axis stator currents, L_D and L_Q are the D axis and Q axis inductances, λ_D and λ_Q are D axis and Q axis stator flux linkages, r_s is the stator resistance, ω_s is the electrical angular velocity, ω_r is the mechanical angular velocity of the rotor, and P is the number of poles.

The electromagnetic torque can be expressed as:

$$T_e = 3P\,[(L_D - L_Q)i_Q i_D\,]\,/\,4 \qquad (6)$$

The equation of the motor dynamics is:

$$T_e = T_l + B\,\omega_r + J\dot{\omega}_r \qquad (7)$$

where T_e is the electromagnetic torque, T_l stands for the load torque, B represents the viscous frictional coefficient,
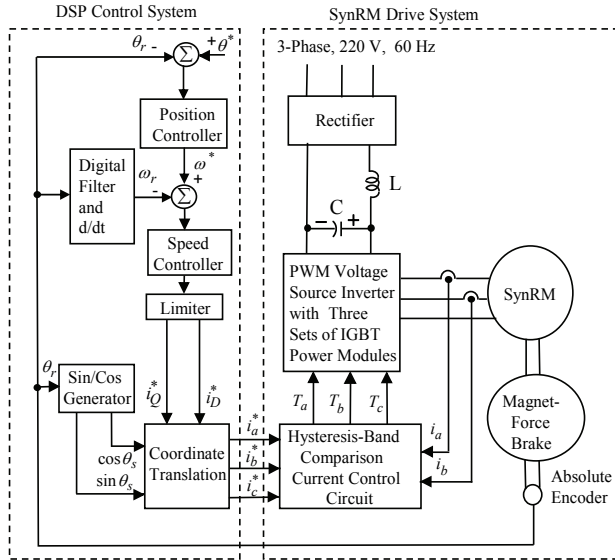
Fig. 1. Configuration of a DSP field-oriented controlled SynRM drive system.

and J is the moment of inertia. The basic principle in controlling a SynRM drive is based on field orientation with a constant current in the d axis. Therefore, the electromagnetic torque T_e is proportional to i_Q, which is determined by the closed-loop control. Since the generated torque is linearly proportional to the q axis current as the d axis rotor flux is constant in (6), the torque per ampere can be achieved. The configuration of a digital signal processor (DSP) field-oriented controlled SynRM drive system is shown in Fig. 1.

The system is constituted by the following parts: a SynRM (loaded with a magnet-force brake machine), a hysteresis-band comparison current-controlled pulse-width-modulation (PWM) voltage source inverter with three sets of insulated-gate-bipolar-transistor (IGBT) power modules, a field-orientation mechanism including a coordinate translator and a $\cos\theta_s / \sin\theta_s$ generator where $\theta_s = P\theta_r / 2$ is the rotating angle of the rotor flux, a speed control loop and a position control loop. For the position control system, the magnet-force brake machine is operated to provide a constant disturbance torque. A mechanism with an adjustable inertia is also coupled to the rotor of the SynRM.

A SynRM drive system with field-oriented control [6-8] can be simplified as the block diagram shown in Fig. 2, where:

$$T_e = k_f i_Q^* \tag{8}$$

$$k_f = \frac{3P}{4}(L_D - L_Q)i_D^* \tag{9}$$

where k_f is the torque constant, i_Q^* is the torque current command, and i_D^* is the field current command to be a constant in the field-oriented control. Moreover, θ_r and
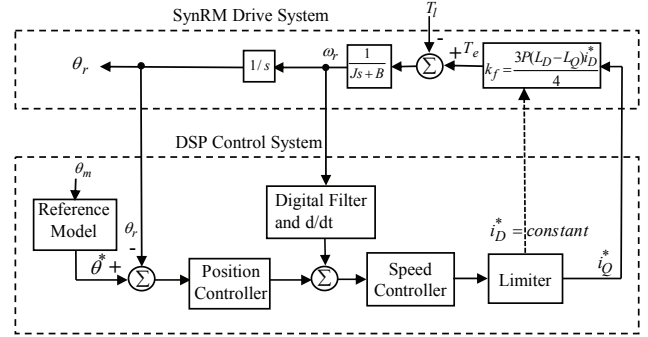

Fig. 2. Simplified block diagram of a field-oriented controlled SynRM drive system.

ω_r are the rotor position and speed. All of the parameters of the SynRM are given as: $J = 1.04 \times 10^{-3} Nms^2$, $B = 6.18 \times 10^{-3} Nms/rad$, $k_f = 0.6527 Nm/A$, $r_s = 1.21 \Omega$, $L_Q = 32.25 mH$, and $L_D = 124.82 mH$. The methods of the electrical parameter identification were used by the open circuit saturation curve, the short circuit current curve, etc. The curve-fitting technique based on the step response of the rotor position is applied to find a model of the drive system under the nominal condition, i.e., $T_l = 0$ Nm without parameter variations. For the convenience of the controller design, the position and speed signals in the control loop are set to 1 V=50 rad and 1 V=50 rad/sec, respectively.

III. CONTROL SYSTEM DESIGN

The uncertainties of an actual SynRM drive system including parameter variations and external load disturbances with nonlinear and time-varying properties are hard to frame in accurate models. The motor dynamics equation (7) including parameter variations and external load disturbances with nonlinear and time-varying properties can be presented as [13]:

$$\dot{q}_1 = f_1 q_1 + g_1 v_1 + h_1 T_l + \Delta f_1 q_1 + \Delta g_1 v_1 \tag{10}$$

where $q_1 = \omega_r = \dot{r}_1 = \dot{\theta}_r$ is the rotor speed of the SynRM, $r_1 = \theta_r$ is the rotor position of the SynRM, $f_1 = -B/J$, $g_1 = k_f/J > 0$, $h_1 = -1/J$, Δf_1 and Δg_1 denote the uncertainties introduced by the system parameters J and B, and v_1 is the control input of the SynRM drive system, i.e., the torque current i_Q. To simplify the equation, (10) is rewritten as [13]:

$$\dot{q}_1 = f_1 q_1 + g_1 v_1 + z_l \tag{11}$$

where $z_l \equiv \Delta f_1 q_1 + \Delta g v_1 + h_1 T_l$ is the lumped uncertainty. The aim of the control system design is to achieve better position tracking performance under nonlinear uncertainty

disturbances for the SynRM drive system. The position tracking error is $d_1 = \theta^* - \theta_r = q_d - r_1$, where $\theta^* = q_d(t)$ is the reference trajectory. The derivative of d_1 is $\dot{d}_1 = \dot{\theta}^* - \dot{\theta}_r = \dot{q}_d - q_1$. The stabilizing function is defined as $c_1 = \dot{q}_d + k_1 d_1 + k_2 d_2$, where k_1 and k_2 are both positive constants. $d_2 = \int d_1(\tau)d\tau$ is the integral function to ensure convergence of the tracking error. The virtual tracking error is defined as $d_3 = q_1 - c_1$. The first Lyapunov function can be opted as $Y_1 = d_1^2 / 2$. Substituting $\dot{d}_1 = \dot{\theta}^* - \dot{\theta}_r = \dot{q}_d - q_1$, $c_1 = q_1 - d_3$ and $c_1 = \dot{q}_d + k_1 d_1 + k_2 d_2$ into the derivative of Y_1 [13] yields:

$$\dot{Y}_1 = d_1 \dot{d}_1 = d_1(\dot{q}_d - q_1) = d_1(\dot{q}_d - c_1 - d_3)$$

$$= -k_1 d_1^2 - k_2 d_1 d_2 - d_1 d_3 \qquad (12)$$

Substituting (10) and the derivative of c_1 into the derivative of d_3 [13] yields:

$$\dot{d}_3 = \dot{q}_1 - \dot{c}_1 = (f_1 q_1 + g_1 v_1 + z_l) - (\ddot{q}_d + k_1 \dot{d}_1 + k_2 \dot{d}_2) \quad (13)$$

The second Lyapunov function can be opted as [13]:

$$Y_2 = Y_1 + k_2 d_2^2 / 2 + d_3^2 / 2 \qquad (14)$$

A. Nonlinear Backstepping Control System Using an Upper Bound with a Switching Function

For designing the proposed nonlinear backstepping control system using an upper bound with a switching function, it is assumed that the lumped uncertainty z_l is bounded, i.e., $|z_l| \le \bar{z}_l$. Substituting d_3, (12), (13), $d_2 = \int d_1(\tau)d\tau$ and the derivative of the integral function into the derivative of (14) yields:

$$\dot{Y}_2 = \dot{Y}_1 + k_2 d_2 \dot{d}_2 + d_3 \dot{d}_3$$

$$= -k_1 d_1^2 - k_2 d_1 d_2 - d_1 d_3 + k_2 d_2 \dot{d}_2$$

$$+ d_3 \{[f_1 q_1 + g_1 v_1 + z_l] - (\ddot{q}_d + k_1 \dot{d}_1 + k_2 \dot{d}_2)\}$$

$$= -k_1 d_1^2 - d_1 d_3 + d_3 \{[f_1 q_1 + g_1 v_1 + z_l] - (\ddot{q}_d + k_1 \dot{d}_1 + k_2 \dot{d}_2)\} \quad (15)$$

Then the nonlinear backstepping control using an upper bound with a switching function $v_1 = i_Q$ can be designed as:

$$v_1 = g_1^{-1}[\ddot{q}_d + k_1 \dot{d}_1 + k_2 \dot{d}_2 + d_1 - f_1 q_1 - \bar{z}_l \,\mathrm{sgn}(d_3) - k_3 d_3] \quad (16)$$

By using the lumped uncertainty bound and substituting (16) into (15), then (15) can be presented as:

$$\dot{Y}_2(d_1, d_2) = -k_1 d_1^2 - k_3 d_3^2 + d_3 z_l - |d_3|\bar{z}_l$$

$$\le -k_1 d_1^2 - k_3 d_3^2 \le 0 \qquad (17)$$

Defining the following function:

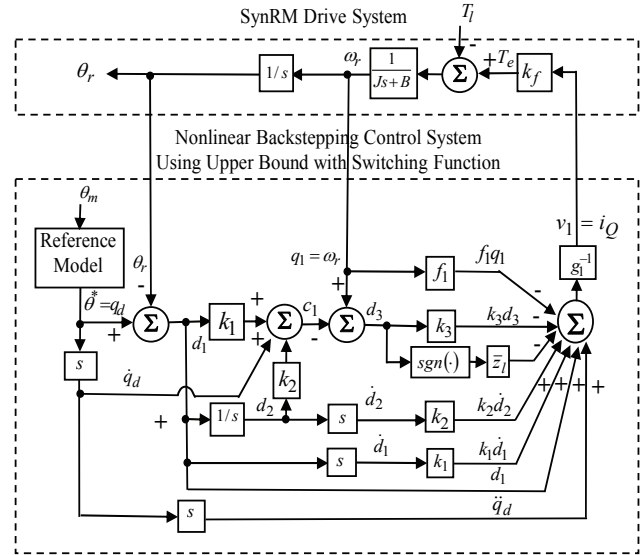$$\rho(t) = k_1 d_1^2 + k_3 d_3^2 \qquad (18)$$

Fig. 3. Block diagram of a nonlinear backstepping control system using am upper bound with a switching function.

Using (17) and the integral (18) yields:

$$\int_0^t \rho(\tau)\, d\tau \le Y_2(d_1(0), d_3(0)) - Y_2(d_1(t), d_3(t)) \quad (19)$$

Since $Y_2(d_1(0), d_3(0))$ is bounded, and $Y_2(d_1(t), d_3(t))$ is non-increasing and bounded, $\lim_{t\to\infty} \int_0^t \rho(\tau)\, d\tau < \infty$. Moreover, $\dot{\rho}(t)$ is bounded, and $\rho(t)$ is uniformly continuous [24], [25]. By using Barbalat's lemma [24], [25], it can be shown that $\lim_{t\to\infty} \rho(t) = 0$. That is d_1 and d_3 converge to zero when $t \to \infty$. In addition, $\lim_{t\to\infty} q_1(t) = \dot{q}_d$ and $\lim_{t\to\infty} r_1 = q_d$. As a result, the stability of the nonlinear backstepping control system using an upper bound with a switching function, as shown in Fig. 3, can be guaranteed.

B. Nonlinear Backstepping Control System Using an Adaptive Law

The proposed nonlinear backstepping control system using an upper bound with a switching function can perform well under general situations. However, when the inertia of the counterweight is varying, this method cannot achieve satisfactory performance. Since the real value of z_l cannot be measured precisely, it is replaced by use of the estimated value $\hat{z}_l$. Therefore, the estimation error can be defined as:

$$\tilde{z}_l = z_l - \hat{z}_l \qquad (20)$$

The third Lyapunov function can be selected as:

$$Y_3 = Y_2 + \tilde{z}_l^2 / (2\beta_1) \qquad (21)$$
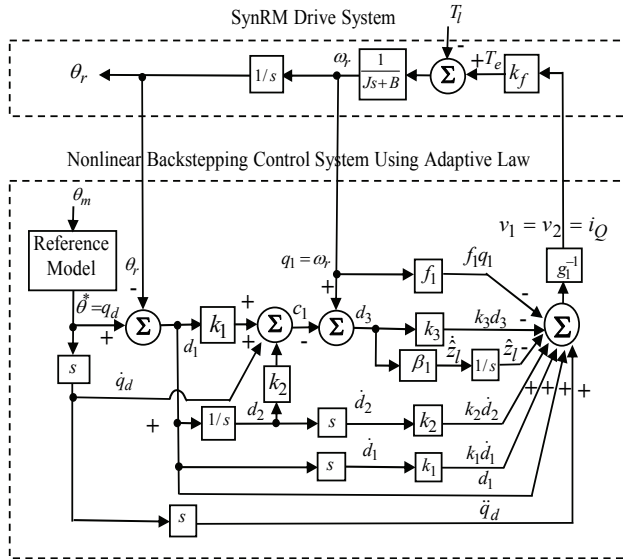
The derivative of (21) is:

Fig. 4. Block diagram of a nonlinear backstepping control system using an adaptive law.

Fig. 5. Architecture of the proposed three-layer reformed recurrent Hermite polynomial neural network.

$$\dot{Y}_3 = \dot{Y}_2 + \tilde{z}_l \, \dot{\tilde{z}}_l \, / \beta_1 = \dot{Y}_2 - \tilde{z}_l \, \dot{\hat{z}}_l \, / \beta_1$$
$$= -k_1 d_1 d_2 - k_2 d_1 d_2 - d_1 d_3 + k_2 d_2 d_2$$
$$+ d_3\{[f_1 q_1 + g_1 v_1 + z_l] - (\ddot{q}_d + k_1 \dot{d}_1 + k_2 \dot{d}_2)\} - \tilde{z}_l \, \dot{\hat{z}}_l \, / \beta_1 \quad (22)$$

Then the nonlinear backstepping control using an adaptive law $v_1 = v_2 = i_Q$ can be designed as:

$$v_1 = v_2 = g_1^{-1}[\ddot{q}_d + k_1 \dot{d}_1 + k_2 \dot{d}_2 + d_1 - f_1 q_1 - \hat{z}_l - k_3 d_3] \quad (23)$$

Taking (23) into (22), then (23) can be presented as:

$$\dot{Y}_3 = \dot{Y}_2 + \tilde{z}_l \, \dot{\tilde{z}}_l \, / \beta_1 = \dot{Y}_2 - \tilde{z}_l \, \dot{\hat{z}}_l \, / \beta_1$$
$$= -k_1 d_1^2 - k_3 \, d_3^2 + d_3 z_l - d_3 \hat{z}_l - \tilde{z}_l \, \dot{\hat{z}}_l \, / \beta_1$$
$$= -k_1 d_1^2 - k_3 \, d_3^2 + d_3 \tilde{z}_l - \tilde{z}_l \, \dot{\hat{z}}_l \, / \beta_1 \quad (24)$$

The adaptive law for $\dot{\hat{z}}_l$ is designed as follows:

$$\dot{\hat{z}}_l = \beta_1 d_3 \quad (25)$$

Taking (25) into (24), then (24) can be rewritten as follows:

$$\dot{Y}_3(d_1, d_2) = -k_1 d_1^2 - k_3 \, d_3^2 \le 0 \quad (26)$$

By using (26), the integral of (18), the bounded and uniformly continuous conditions, and Barbalat's lemma [24], [25], it can be shown that $\lim_{t \to \infty} \rho(t) = 0$. That is, d_1 and d_3 converge to zero when $t \to \infty$. Moreover, $\lim_{t \to \infty} q_1(t) = \dot{q}_d$ and $\lim_{t \to \infty} r_1 = q_d$. As a result, the stability of the nonlinear backstepping control using an adaptive law, as shown in Fig. 4, can be guaranteed.
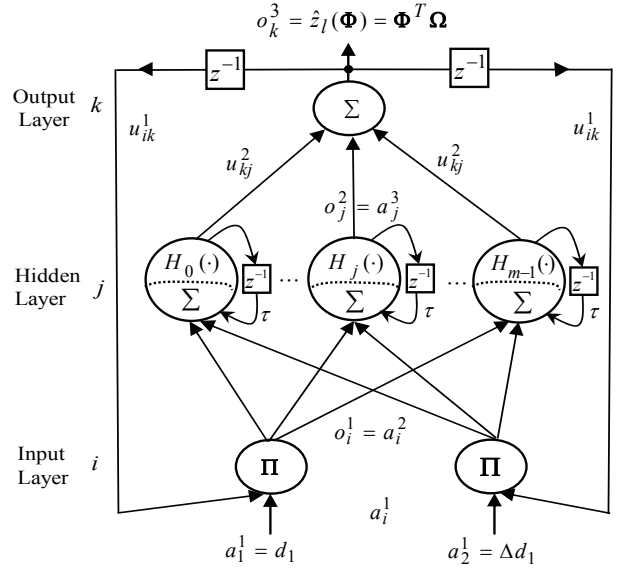
C. Nonlinear Backstepping Control System Using a Reformed Recurrent Hermite Polynomial Neural Network with an Adaptive Law and an Error Estimated Law

Because lumped uncertainty z_l is unknown in practical applications, it is difficult to determine the upper bound $\bar{z}_l$. Therefore, it will be observed by an adaptive uncertainty observer and assumed to be constant during the observation. The above assumption is valid in the practical digital processing of the observer since the sampling period of the observer is short enough when compared with the variation of z_l. A reformed recurrent Hermite polynomial neural network is proposed to adapt the value of the lumped uncertainty z_l. The architecture of the proposed three-layer reformed recurrent Hermite polynomial neural network is depicted in Fig. 5. It is composed of an input layer (the i layer), a hidden layer (the j layer) and an output layer (the k layer). The activation functions and signal actions of the nodes in each layer of the reformed recurrent Hermite polynomial neural network are described as follows:

Layer 1: Input Layer

Each node i in this layer is indicated by $\prod$, which multiplies them by each other or between each other for input signals. Then the outputs signals are the result of the product. The input and the output for all of the nodes i in this layer are expressed as:

$$nd_i^1(N) = \prod_k a_i^1(N) u_{ik}^1 \, o_k^3(N-1),$$
$$o_i^1(N) = l_i^1(nd_i^1(N)) = nd_i^1(N), \quad i = 1, 2 \quad (27)$$

The first input signal $a_1^1 = d_1$ is the tracking error between the desired rotor position θ^* and the actual rotor position θ_r. The second input signal $a_2^1 = d_1(1-z^{-1}) = \Delta d_1$ is the tracking error increment. N denotes the number of iterations. The connecting weights u_{ik}^1 are the recurrent weights between the output layer and the input layer. o_i^1 is the output value from the input layer of the reformed recurrent Hermite polynomial neural network. o_k^3 is the output value from the output layer of the reformed recurrent Hermite polynomial neural network.

Layer 2: Hidden Layer
The single node jth in this layer is labeled as Σ . The net input and the net output for node jth of the hidden layer are expressed as:

$$nd_j^2(N) = \sum_{i=1}^{2} o_i^1(N) + \tau o_j^2(N-1),$$

$$o_j^2(N) = l_j^2(nd_j^2(N)) = H_j(nd_j^2(N)), \quad j = 0,1,2,\cdots,(m-1) \qquad (28)$$

where τ , which is selected between 0 and 1, is the self-feedback gain of the hidden layer. The Hermite polynomials [20-23] $H_n(x)$ are the arguments of the polynomials with $-1<x<1$, and n is the order of expansion. m is the number of nodes. The zero, first and second order Hermite polynomials are given by $H_0(x)=1$, $H_1(x)=2x$ and $H_2(x)=4x^2-2$, respectively. Higher order Hermite polynomials may be generated by the recursive formula $H_{n+1}(x)=2xH_n(x)-2nH_{n-1}(x)$.

Layer 3: Output Layer
The node kth in this layer is labeled as Σ . It is the summation of all of the input signals. The net input and the net output for node kth in this layer can be expressed as:

$$nd_k^3(N) = \sum_{j=0}^{m-1} u_{kj}^2 o_j^2(N),$$

$$o_k^3(N) = l_k^3(nd_k^3(N)) = nd_k^3(N), \quad k=1 \qquad (29)$$

where u_{kj}^2 is the connective weight between the hidden layer and the output layer, l_k^3 is the activation function that is selected as a linear function, and l_i^1 and l_k^3 are the activation function which is selected as a linear function.

$o_j^2(N)$ represents the jth input to the node of the output layer. The output value $o_k^3(N)$ of the reformed recurrent Hermite polynomial neural network can be indicated as:

$$o_k^3(N) = \hat{z}_l(\Phi) = \Phi^T \Omega \qquad (30)$$

where $\Phi = \begin{bmatrix} u_{01}^2 & u_{11}^2 & \cdots & u_{m-1,1}^2 \end{bmatrix}^T$ is a collection of the adjustable parameters of the reformed recurrent Hermite polynomial

neural network. $a_j^3(N) = o_j^2(N)$ represents the jth input to the node of the output layer. $\Omega = \begin{bmatrix} a_0^3 & a_1^3 & \cdots & \cdots & a_{m-1}^3 \end{bmatrix}^T$, where o_j^2 is determined by the selected Hermite polynomials and $0 \leq o_j^2 \leq 1$.

The minimum reconstructed error e can be defined as follows:

$$e = z_l - z_l(\Phi^*) = z_l - (\Phi^*)^T \Omega \qquad (31)$$

where Φ^* is the optimal weight vector that achieves the minimum reconstructed error, and the absolute value of e is assumed to be less than a small positive constant $\bar{e}$, i.e., $|e| \leq \bar{e}$. To develop the adaptive law of the reformed recurrent Hermite polynomial neural network and an error estimated law, a Lyapunov candidate is chosen as:

$$Y_3 = Y_2 + (\hat{e}-e)^2/(2\gamma) + (\Phi-\Phi^*)^T(\Phi-\Phi^*)/(2\eta_1) \qquad (32)$$

where γ and η_1 are positive constants, and $\hat{e}$ is the estimated value of the minimum reconstructed error e. The estimation value $\hat{e}$ of the reconstructed error e is to compensate the observed error induced by the reformed recurrent Hermite polynomial neural network uncertainty observer and to guarantee the stable characteristic of the whole control system. Take the derivative of Y_3 as:

$$\dot{Y}_4 = \dot{Y}_2 + (\hat{e}-e)\dot{\hat{e}}/\gamma + (\Phi-\Phi^*)^T\dot{\Phi}/\eta_1$$
$$= -k_1 d_1^2 - k_2 d_1 d_2 - d_1 d_3 + k_2 d_2 \dot{d}_2 + d_3\{[f_1(c_1+d_3) + g_1 v_1 + z_l]\}$$
$$- d_3\{(\ddot{q}_d + k_1 \dot{d}_1 + k_2 \dot{d}_2)\} + (\hat{e}-e)\dot{\hat{e}}/\gamma + (\Phi-\Phi^*)^T\dot{\Phi}/\eta_1 \quad (33)$$

According to (33), an adaptive laws for $\dot{\Phi}$ and an error estimated law $\dot{\hat{e}}$ are designed as follows:

$$\dot{\Phi} = \eta_1 d_3 \Omega \qquad (34)$$

$$\dot{\hat{e}} = \gamma d_3 \qquad (35)$$

Then the nonlinear backstepping control using the reformed recurrent Hermite polynomial neural network with an adaptive law and an error estimated law $v_1 = v_3 = i_Q$ is proposed as follows:

$$v_1 = v_3 = g_1^{-1}[\ddot{q}_d + k_1 \dot{d}_1 + k_2 \dot{d}_2 + d_1 - f_1 q_1 - \hat{e} - \hat{z}_l - k_3 d_3] \quad (36)$$

By substituting (36) into (33) and using (31), then (33) can be rewritten as:

$$\dot{Y}_4 = -k_1 d_1^2 - k_3 d_3^2 + d_3 z_l - d_3 \hat{z}_l - d_3 \hat{e}$$
$$+ (\hat{e}-e)\dot{\hat{e}}/\gamma + (\Phi-\Phi^*)^T\dot{\Phi}/\eta_1$$
$$= -k_1 d_1^2 - k_3 d_3^2 - d_3 \hat{e} + d_3(z_l - z_l(\Phi^*)) - d_3(\hat{z}_l(\Phi) - z_l(\Phi^*))$$
$$+ (\hat{e}-e)\dot{\hat{e}}/\gamma + (\Phi-\Phi^*)^T\dot{\Phi}/\eta_1$$
$$= -k_1 d_1^2 - k_3 d_3^2 - d_3(\hat{e}-e) - d_3(\Phi-\Phi^*)^T\Omega \qquad (37)$$
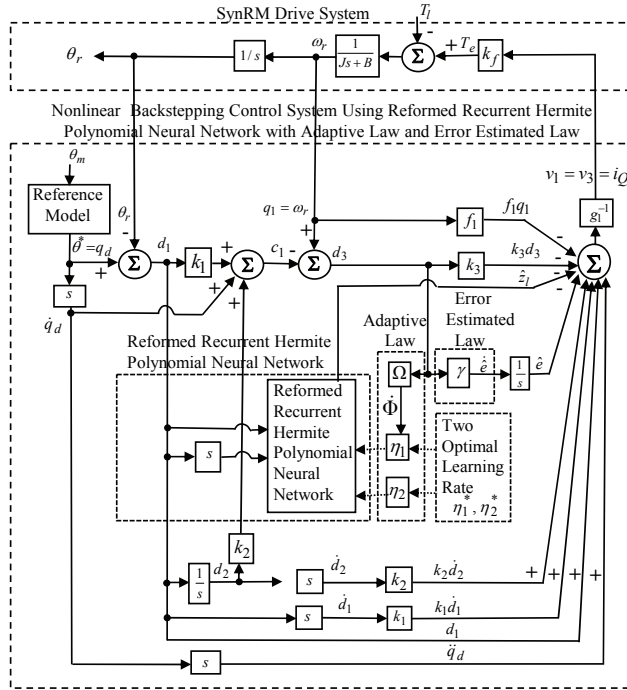$$+ (\hat{e}-e)\dot{\hat{e}}/\gamma + (\Phi-\Phi^*)^T\dot{\Phi}/\eta_1$$

Fig. 6. Block diagram of a nonlinear backstepping control system using the reformed recurrent Hermite polynomial neural network with an adaptive law and an error estimated law.

By substituting (34) and (35) into (37), then (37) can be rewritten as follows:

$$\dot{Y}_4(d_1, d_2) = -k_1 d_1^2 - k_3\, d_3^2 \le 0 \tag{38}$$

By using (38), the integral of (18), the bounded and uniformly continuous conditions, and Barbalat's lemma [24], [25], it can be shown that $\lim_{t \to \infty} \rho(t) = 0$. That is d_1 and d_3 converge to zero when $t \to \infty$. Moreover, $\lim_{t \to \infty} q_1(t) = \dot{q}_d$ and $\lim_{t \to \infty} r_1 = q_d$. As a result, the stability of the nonlinear backstepping control using the reformed recurrent Hermite polynomial neural network with an adaptive law and an error estimated law, as shown in Fig. 6, can be guaranteed. On the other hand, guaranteed convergence of the tracking error to zero does not imply convergence of the estimated value of the lumped uncertainty to its real values. The persistent excitation condition [25] should be satisfied for the estimated value to converge to its theoretic value.

D. On-Line Training Algorithm of the Reformed Recurrent Hermite Polynomial Neural Network

In order to describe the on-line training algorithm of the reformed recurrent Hermite polynomial neural network, a cost function is defined as [26], [27]:

$$X_1 = d_3^2 / 2 \tag{39}$$

The adaptive law of the connective weight using the gradient descent method can be represented as:

$$\dot{u}_{kj}^2 = \eta_1\, d_3 \mathbf{\Omega} \underline{\Delta} - \eta_1 \frac{\partial X_1}{\partial o_k^3} \frac{\partial o_k^3}{\partial u_{kj}^2} = -\eta_1 \frac{\partial X_1}{\partial o_k^3} o_j^2 \tag{40}$$

The above Jacobian term of the controlled system can be rewritten as $\partial X_1 / \partial o_k^3 = -d_3$. The recurrent weight u_{ik}^1 from the Jacobian term of the controlled system is updated as:

$$\dot{u}_{ik}^1 \equiv -\eta_2 \frac{\partial X_1}{\partial u_{ik}^1} = -\eta_2 \frac{\partial X_1}{\partial o_k^3} \frac{\partial o_k^3}{\partial\, o_j^2} \frac{\partial o_j^2}{\partial\, o_i^1} \frac{\partial o_i^1}{\partial u_{ik}^1} \tag{41}$$

$$= \eta_2\, d_3 u_{kj}^2 H_j(\cdot) a_i^1(N) o_k^3(N-1)$$

E. Two Optimal Learning Rate Derivations and a Convergence Analysis of the Reformed Recurrent Hermite Polynomial Neural Network

Two optimal learning rates are derived to assure the convergence of the output tracking error. In addition, a convergence analysis is provided in the following two theorems.

Theorem 1: Assume that η_1 is the learning rate of the connective weight between the hidden layer and the output layer in the reformed recurrent Hermite polynomial neural network. Meanwhile, let R_{1max} be defined as $R_{1max} \equiv max_N \|R_1(N)\|$, where $R_1(N) = \partial o_k^3 / \partial u_{kj}^2$ and $\|\cdot\|$ is the Euclidean norm in $\Re^n$. In addition, η_1 is chosen as [26], [27]:

$$0 < \eta_1 < 2 / (R_{1\,max})^2 \tag{42}$$

The convergence of the output tracking error is guaranteed. Furthermore, the optimal learning rate, which achieves fast convergence, can be obtained as:

$$\eta_1^* = 1 / [(R_{1\,max})^2] \tag{43}$$

Proof: Since:

$$R_1(N) = \frac{\partial o_k^3}{\partial u_{kj}^2} = o_j^2 \tag{44}$$

A Lyapunov function can be selected as:

$$Y_5(N) = \frac{1}{2} d_3^2(N) \tag{45}$$

The increment in the Lyapunov function can be depicted as:

$$\Delta Y_5(N) = Y_5(N+1) - Y_5(N) = \frac{1}{2}\left[d_3^2(N+1) - d_3^2(N)\right] \tag{46}$$

Then the error difference can be represented by:

$$d_3(N+1) = d_3(N) + \Delta d_3(N) = d_3(N) + \left[\frac{\partial d_3(N)}{\partial u_{kj}^2}\right]^T \Delta u_{kj}^2 \tag{47}$$

where $\Delta d_3(N)$ is the output error increment, and Δu_{kj}^2 represents increment of the weight. By using (39), (40) and (44), then (47) can be obtained as:

$$\frac{\partial d_3(N)}{\partial u_{kj}^2} = \frac{\partial d_3(N)}{\partial X_1}\frac{\partial X_1}{\partial o_k^3}\frac{\partial o_k^3}{\partial u_{kj}^2} = -\frac{d_3}{d_3(N)}R_1(N) \qquad (48)$$

$$d_3(N+1) = d_3(N) - \left[\frac{d_3}{d_3(N)}R_1(N)\right]^T \eta_1\, d_3 R_1(N) \qquad (49)$$

Thereby:

$$\|d_3(N+1)\| = \left\|d_3(N)\left[1 - \eta_1(d_3/d_3(N))^2 R_1^T(N)R_1(N)\right]\right\|$$

$$\leq \|d_3(N)\|\left\|1 - \eta_1(d_3/d_3(N))^2 R_1^T(N)R_1(N)\right\| \qquad (50)$$

By using (46), (47), (48), (49) and (50), then $\Delta Y_4(N)$ can be rewritten as:

$$\Delta Y_4(N) = \frac{1}{2}\eta_1[d_3]^2 R_1^T(N)R_1(N)$$
$$\cdot\left\{\eta_1[d_3/d_3(N)]^2 R_1^T(N)R_1(N) - 2\right\}$$
$$\leq \frac{1}{2}\eta_1[d_3]^2\left(R_{1\max}(N)\right)^2\left\{\eta_1[d_3/d_3(N)]^2\left(R_{1\max}(N)\right)^2 - 2\right\} \qquad (51)$$

If η_1 is chosen as $0 < \eta_1 < 2/\{(R_{1\max})^2[d_3/d_3(N)]^2\}$, the Lyapunov stability of $Y_5(N) > 0$ and $\Delta Y_5 < 0$ is guaranteed. Then the output tracking error converges to zero as $t \to \infty$. This completes the proof of the theorem. Furthermore, the optimal learning rate, which achieves fast convergence, corresponds to [26], [27]:

$$2\eta_1^*\{(R_{1\max})^2[d_3/d_3(N)]^2\} - 2 = 0 \qquad (52)$$

i.e.:

$$\eta_1^* = 1/\{(R_{1\max})^2[d_3/d_3(N)]^2\} = 1/(R_{1\max})^2 \qquad (53)$$

which comes from the derivative of (51) with respect to η_1 and is equal to zero. This shows interesting results for the optimal learning rate which can be on-line tuned at each instant.

Theorem 2: Assume that η_2 is the learning rate of the recurrent weight between the output layer and the input layer in the reformed recurrent Hermite polynomial neural network. Meanwhile, let $R_{2\max}$ be defined as $R_{2\max} \equiv \max_N \|R_2(N)\|$, where $R_2(N) = \partial o_k^3/\partial u_{ik}^1$ and $\|\cdot\|$ is the Euclidean norm in $\Re^n$. If η_2 is chosen as [26], [27]:

$$0 < \eta_2 < 2/(R_{2\max})^2 \qquad (54)$$

Then the convergence of the output tracking error is guaranteed. Furthermore, the optimal learning rate which achieves the fast convergence can be obtained as:

$$\eta_2^* = 1/(R_{2\max})^2 \qquad (55)$$

Proof: Since:

$$R_2(N) = \frac{\partial o_k^3}{\partial u_{ik}^1} = u_{kj}^2 H_j(\cdot)a_i^1(N)o_k^3(N-1) \qquad (56)$$

The Lyapunov function can be selected as (45) and the increment in the Lyapunov function can be depicted as (46).

Then the error difference can be depicted as:

$$d_3(N+1) = d_3(N) + \Delta d_3(N) = d_3(N) + \left[\frac{\partial d_3(N)}{\partial u_{ik}^1}\right]^T \Delta u_{ik}^1 \qquad (57)$$

where Δu_{ik}^1 represents the increment of the weight. By using (39), (41) and (56), then (57) can be depicted as:

$$\frac{\partial d_3(N)}{\partial u_{ik}^1} = \frac{\partial d_3(N)}{\partial X_1}\frac{\partial X_1}{\partial o_k^3}\frac{\partial o_k^3}{\partial u_{ik}^1} = -\frac{d_3}{d_3(N)}R_2(N) \qquad (58)$$

$$d_3(N+1) = d_3(N) - \left[\frac{d_3}{d_3(N)}R_2(N)\right]^T \eta_2\, d_3 R_2(N) \qquad (59)$$

Thereby:

$$\|d_3(N+1)\| = \left\|d_3(N)\left[1 - \eta_2(d_3/d_3(N))^2 R_2^T(N)R_2(N)\right]\right\|$$

$$\leq \|d_3(N)\|\left\|1 - \eta_2(d_3/d_3(N))^2 R_2^T(N)R_2(N)\right\| \qquad (60)$$

By using (46), (57), (58), (59) and (60), the $\Delta Y_5(N)$ can be rewritten as:

$$\Delta Y_5(N) = \frac{1}{2}\eta_2[d_3]^2 R_2^T(N)R_2(N)$$
$$\cdot\left\{\eta_2[d_3/d_3(N)]^2 R_2^T(N)R_2(N) - 2\right\}$$
$$\leq \frac{1}{2}\eta_2[d_3]^2\left(R_{2\max}(N)\right)^2\left\{\eta_2[d_3/d_3(N)]^2\left(R_{2\max}(N)\right)^2 - 2\right\} \qquad (61)$$

If η_2 is chosen as $0 < \eta_2 < 2/\{(R_{2\max})^2[d_3/d_3(N)]^2\}$, then the Lyapunov stability of $Y_5(N) > 0$ and $\Delta Y_5 < 0$ is guaranteed. Therefore, the output tracking error converges to zero as $t \to \infty$. This completes the proof of the theorem. Moreover, the optimal learning rate, which achieves a fast convergence, corresponds to [26], [27]:

$$2\eta_2^*\{(R_{2\max})^2[d_3/d_3(N)]^2\} - 2 = 0 \qquad (62)$$

i.e.:

$$\eta_2^* = 1/\{(R_{2\max})^2[d_3/d_3(N)]^2\} = 1/\{(R_{2\max})^2\} \qquad (63)$$

which comes from the derivative of (61) with respect to η_2 and is equal to zero. This shows interesting results for the optimal learning rate, which can be on-line tuned at each instant.

In summary, the online tuning algorithm of the reformed recurrent Hermite polynomial neural network is based on adaptive laws (40) and (41) for the connective weight adjustment and the recurrent weights adjustment with the two optimal learning rates in (43) and (55), respectively. Moreover, the reformed recurrent Hermite polynomial neural network weight estimation errors are fundamentally bounded [28]. In addition, the control signal is bounded.

Fig. 7. Photo of the experimental set-up.

IV. EXPERIMENTAL RESULTS

A block diagram of a SynRM drive system is depicted in Fig. 1. A photo of the experimental set-up is shown in Fig. 7.

The proposed controllers are implemented by a DSP control system. The DSP control board includes 4-channels of D/A converter and 2-channels of encoder interface circuits. The coordinate translation in the field-oriented mechanism is implemented by the DSP control system. The SynRM used in this drive system is a three-phase two-pole 230 V, 375 W, 2.7 A, 3600 rpm type. For the position control system, a magnet-force brake machine is operated to provide a constant disturbance torque. A mechanism with an adjustable inertia is also coupled to the rotor of the SynRM. The sampling interval of the control processing in the experiment is set at 2 $m$sec. The methodologies proposed for the real-time control implementation in the DSP are composed of a main program and a secondary interrupt service routine (SIR) in the DSP control system as shown in Fig. 8.

In the main program, the parameters and input/output (I/O) initialization are processed first. Then the interrupt interval for the SIR is set. After enabling the interrupt, the main program is used to monitor the control data. A SIR with a 2 $m$sec sampling interval is used for reading the rotor position of the SynRM drive system from the encoder and three-phase currents of the A/D converter, calculating the reference model and position error, executing the lookup table and coordinate translation, executing the nonlinear backstepping control system using the reformed recurrent Hermite polynomial neural network with an adaptive law and an error estimated law, and outputting three-phase current commands to the hysteresis-band comparison current control circuit for switching the PWM voltage source inverter with three sets of IGBT power modules via interlock and isolated circuits. The PWM voltage source inverter with three sets of IGBT power modules is executed by current-controlled sinusoidal PWM with a switching frequency of 15 kHz by means of a triangular carrier wave. In addition, the measured bandwidth of the speed control loop is about 200Hz and the measured
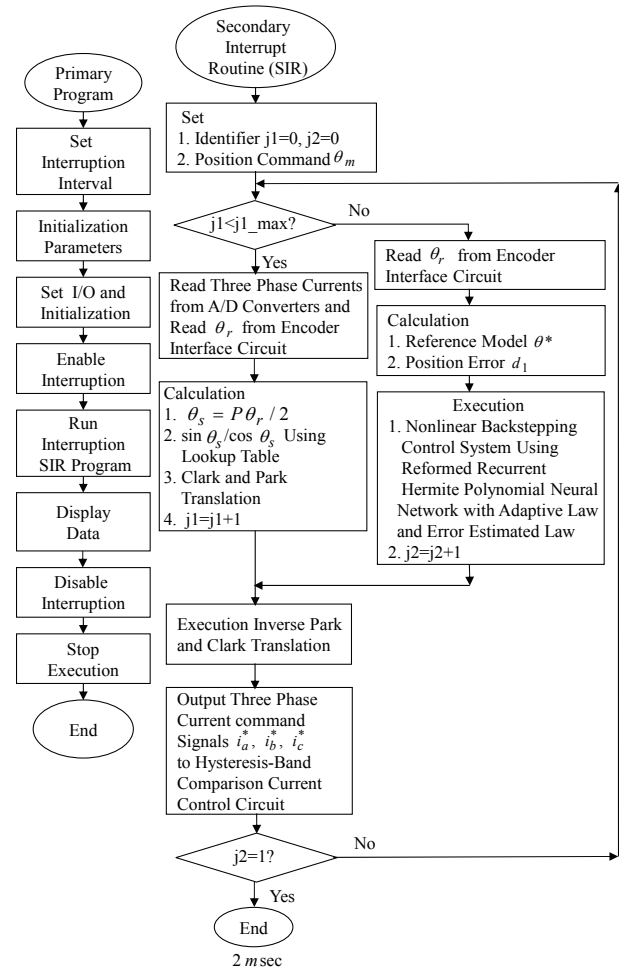

Fig. 8. Flowchart of the executing program using a DSP control system.

bandwidth of the current control loop is about 2000Hz for the SynRM drive system during a no-load test.

Five test cases are provided for control performance comparisons between the conventional PI controller, the proposed nonlinear backstepping control system using an upper bound with a switching function, the proposed nonlinear backstepping control system using an adaptive law, and the proposed nonlinear backstepping control system using the reformed recurrent Hermite polynomial neural network with an adaptive law and an error estimated law. Case 1 is a periodic step command from 0 rad to 6.28 rad in the nominal case. Case 2 is a periodic step command from 0 rad to 6.28 rad in the parameter disturbance case with 4 times the nominal value as an increasing of the rotor inertia and viscous friction. Case 3 is a periodic sinusoidal command from -6.28 rad to 6.28 rad in the nominal case. Case 4 is a periodic sinusoidal command from -6.28 rad to 6.28 rad in the parameter disturbance case with 4 times the nominal value as an increasing of the rotor inertia and viscous friction. Case 5 is a load torque disturbance $T_l = 2 \ Nm$ while adding load case. To achieve good transient and steady-state control
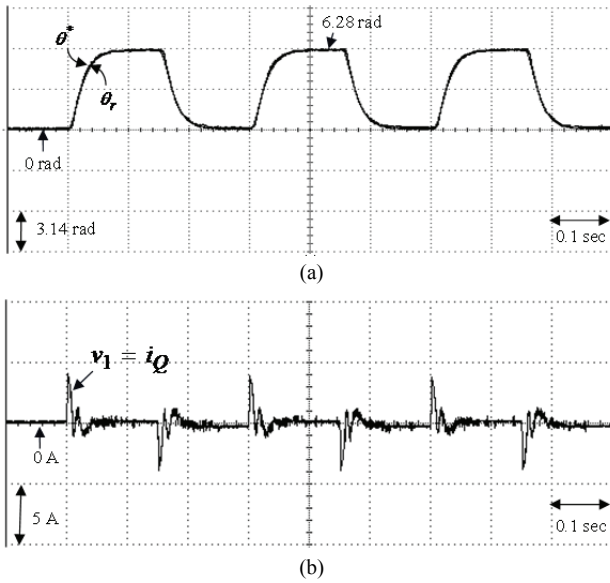
(a)

(b)

Fig. 9. Experimental results of the conventional PI controller attributed to Case 1: (a) Position response of the rotor, (b) Response of the control effort, i.e., torque current i_Q .
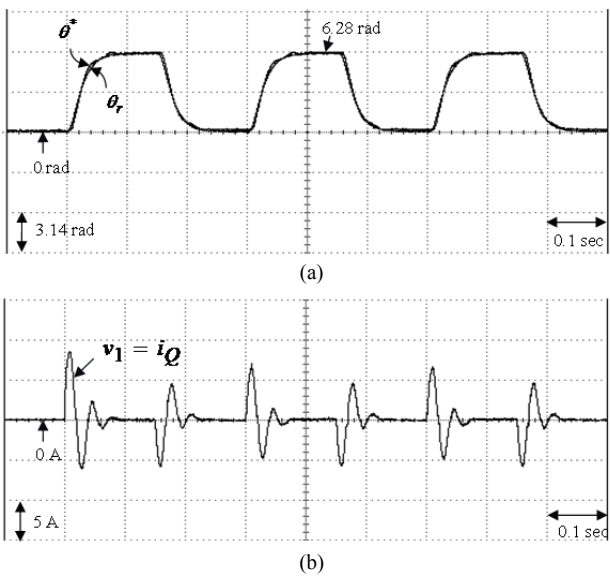

(a)

(b)

Fig. 10. Experimental results of the conventional PI controller attributed to Case 2: (a) Position response of the rotor, (b) Response of the control effort, i.e., torque current i_Q .

performance, all of the gains of the conventional PI controller are $k_{pp} = 5.5$, $k_{ip} = k_{pp}/T_{ip} = 2.8$ through heuristic knowledge [29]-[31] on the tuning of the PI controller attributed to Case 1 for position tracking. In this way, good transient and steady-state control performance is achieved. First, a second-order transfer function in the following form with a rising time of 0.05 sec is chosen as the reference model [32] by using a reduction of the order method for the periodic step command:

$$\left.\frac{\theta^*(s)}{\theta_m(s)}\right|_{T_l=0} = \frac{1156}{s^2 + 68s + 1156} \tag{64}$$

Then when the command is a sinusoidal reference trajectory, the reference model is set as a unit gain. Experimental results obtained with the conventional PI controller for controlling the SynRM drive system attributed to Case 1 and Case 2 are shown in Figs. 9 and 10, respectively. The position responses of the rotor attributed to Case 1 and Case 2 are shown in Figs. 9(a) and 10(a), respectively. In addition, the associated control efforts, i.e., torque current i_Q , are shown in Figs. 9(b) and 10(b), respectively. Experimental results obtained with the conventional PI controller for controlling the SynRM drive system attributed to Case 3 and Case 4 are shown in Figs. 11 and 12, respectively. The position responses of the rotor attributed to Case 3 and Case 4 are shown in Figs. 11(a) and 12(a), respectively. In addition, the associated control efforts, i.e., torque current i_Q , are shown in Figs. 11(b) and 12(b), respectively.

Favorable tracking responses of the position can be obtained by using the conventional PI controller in Case 1 and Case 3 as shown in Figs. 9(a) and 11(a). Moreover, the two worsened tracking responses of the position, shown in Figs. 10(a) and 12(a), are very obvious due to the bigger nonlinear disturbance. From these experimental results, sluggish tracking responses of the position are obtained for controlling the SynRM drive system using the conventional PI controller. The linear controller has weak robustness under bigger nonlinear disturbance since it has no appropriately gains tuning or large nonlinear effect.

The parameters of the proposed nonlinear backstepping control system using an upper bound with a switching function are given as $k_1 = 2.2$, $k_2 = 1.7$, $k_3 = 2.3$ and $\bar{z}_l = 7.5$ according to heuristic knowledge [11], [12], which results in a periodic step command from 0 rad to 6.28 rad in the nominal case for the position tracking to achieve good transient and steady-state control performances. Experimental results obtained with the proposed nonlinear backstepping control system using an upper bound with a switching function for controlling the SynRM drive system attributed to Case 1 and Case 2 are shown in Figs. 13 and 14, respectively.

The position responses of the rotor attributed to Case 1 and Case 2 are shown in Figs. 13(a) and 14(a), respectively. The associated control efforts, i.e., torque current i_Q , are shown in Figs. 13(b) and 14(b), respectively.

Experimental results of the proposed nonlinear backstepping control system using an upper bound with a switching function for controlling the SynRM drive system attributed to Case 3 and Case 4 are shown in Figs. 15 and 16, respectively. The position responses of the rotor attributed to Case 3 and Case 4 are shown in Figs. 15(a) and 16(a), respectively. The associated control efforts, i.e., torque current i_Q , are shown in Figs. 15(b) and 16(b), respectively. Favorable tracking
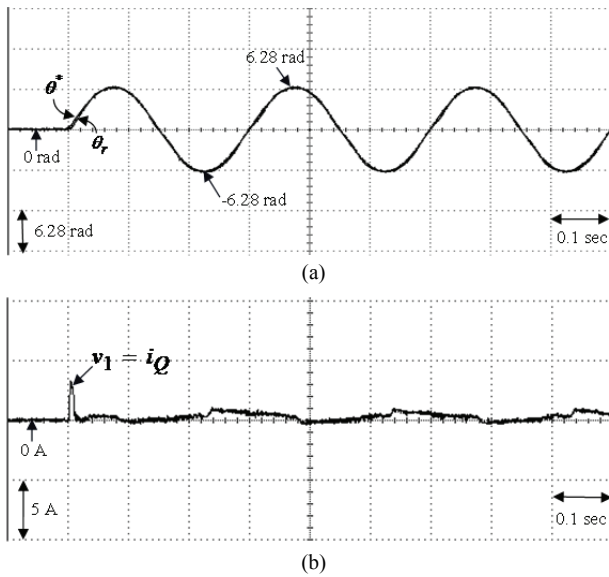
(a)

(b)

Fig. 11. Experimental results of the conventional PI controller attributed to Case 3: (a) Position response of the rotor, (b) Response of the control effort, i.e., torque current i_Q.
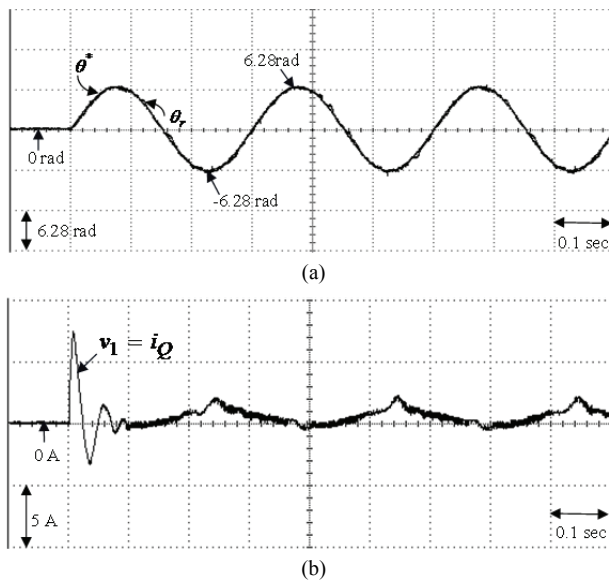

(a)

(b)

Fig. 12. Experimental results of the conventional PI controller attributed to Case 4: (a) Position response of the rotor, (b) Response of the control effort, i.e., torque current i_Q.

(a)

(b)

Fig. 13. Experimental results obtained with the proposed nonlinear backstepping control system using an upper bound with a switching function attributed to Case 1: (a) Position response of the rotor, (b) Response of the control effort, i.e., torque current i_Q.

(a)

(b)

Fig. 14. Experimental results obtained with the proposed nonlinear backstepping control system using an upper bound with a switching function attributed to Case 2: (a) Position response of the rotor, (b) Response of the control effort, i.e., torque current i_Q.

responses of the position can be obtained by means of the proposed nonlinear backstepping control system using an upper bound with a switching function under Case 1 and Case 3 as shown in Figs. 13(a) and 15(a), respectively. Meanwhile, fine tracking responses of the position shown in Figs. 14(a) and 16(a) are obvious under bigger nonlinear disturbance. From these experimental results, good tracking responses of the position are obtained for controlling the SynRM drive system by means of the proposed nonlinear backstepping control system using an upper bound with a switching function under the nominal case and the parameter
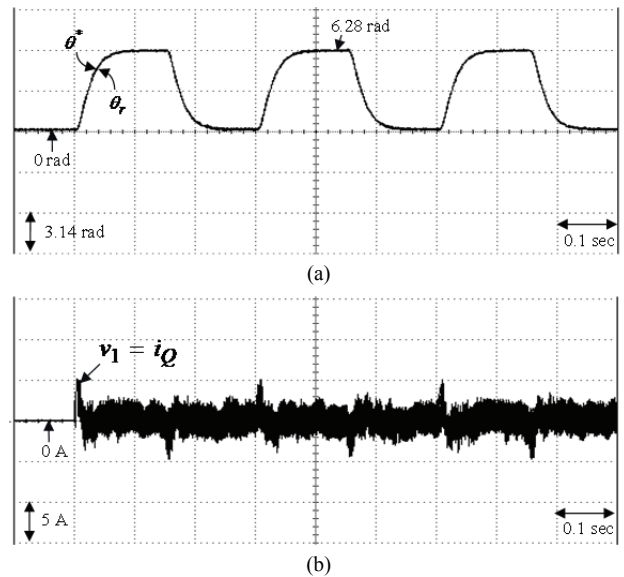
disturbance case. However, a larger upper bound with a switching function results in very serious chattering in the control effort, i.e., torque current i_Q. Moreover, the chattering control effort produces wear on the bearing mechanism and may excite unstable system dynamics.

The parameters of the nonlinear backstepping control system using an adaptive law are given as $k_1 = 2.2$, $k_2 = 1.7$,
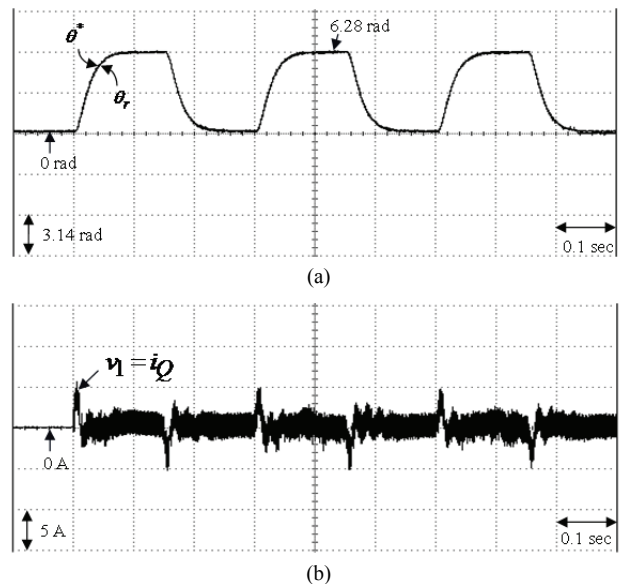
(a)

(b)

Fig. 15. Experimental results obtained with the proposed nonlinear backstepping control system using an upper bound with a switching function attributed to Case 3: (a) Position response of the rotor, (b) Response of the control effort, i.e., torque current i_Q.

(a)

(b)

Fig. 17. Experimental results obtained with the proposed nonlinear backstepping control system using an adaptive law attributed to Case 1: (a) Position response of the rotor, (b) Response of the control effort, i.e., torque current i_Q.
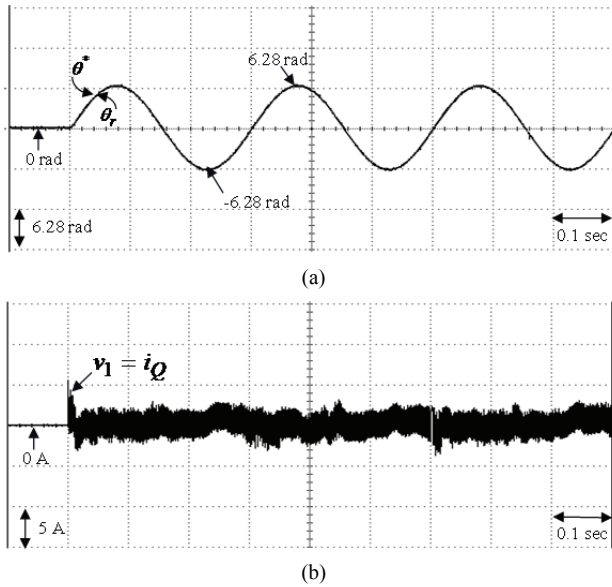

(a)

(b)

Fig. 16. Experimental results obtained with the proposed nonlinear backstepping control system using an upper bound with a switching function attributed by Case 4: (a) Position response of the rotor, (b) Response of the control effort, i.e., torque current i_Q.
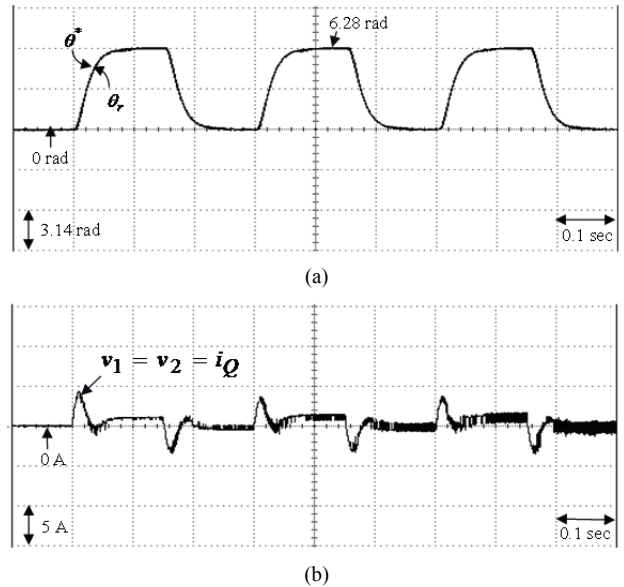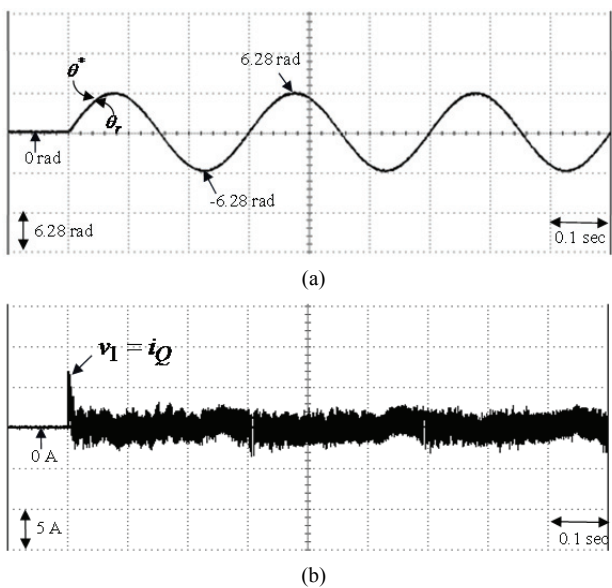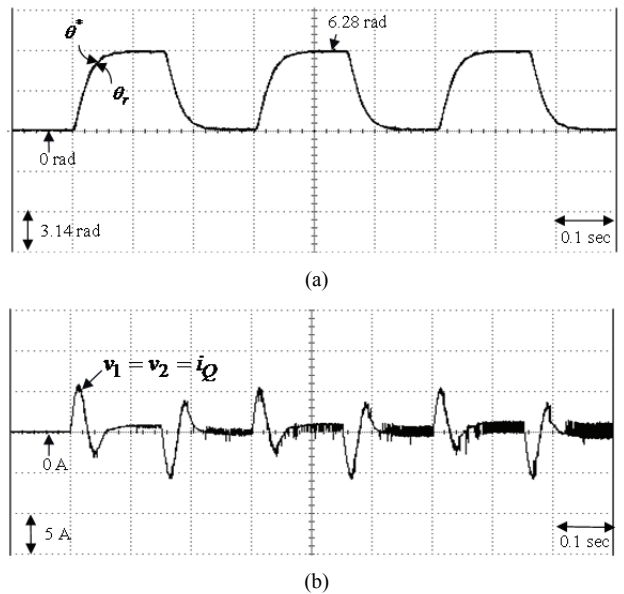

(a)

(b)

Fig. 18. Experimental results obtained with the proposed nonlinear backstepping control system using an adaptive law attributed to Case 2: (a) Position response of the rotor, (b) Response of the control effort, i.e., torque current i_Q.

$k_3 = 2.3$ and $\beta_1 = 0.52$ according to heuristic knowledge [11], [12], which results in a periodic step command from 0 rad to 6.28 rad in the nominal case for the position tracking to achieve good transient and steady-state control performances. Experimental results of the proposed nonlinear backstepping control system using an adaptive law for controlling the SynRM drive system attributed to Case 1 and Case 2 are

shown in Fig. 17 and Fig. 18, respectively. The position responses of the rotor under Case 1 and Case 2 are shown in Figs. 17(a) and 18(a), respectively. In addition, the associated control efforts, i.e., torque current i_Q, are shown in Figs. 17(b) and 18(b), respectively. Experimental results of the proposed nonlinear backstepping control system using an adaptive law for controlling the SynRM drive system attributed to Case 3 and Case 4 are shown in Fig. 19 and
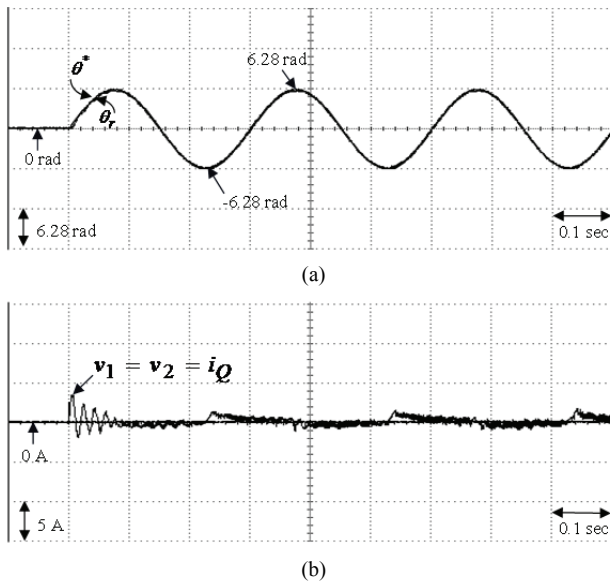
(a)

(b)

Fig. 19. Experimental results obtained with the proposed nonlinear backstepping control system using an adaptive law attributed to Case 3: (a) Position response of the rotor, (b) Response of the control effort, i.e., torque current i_Q.
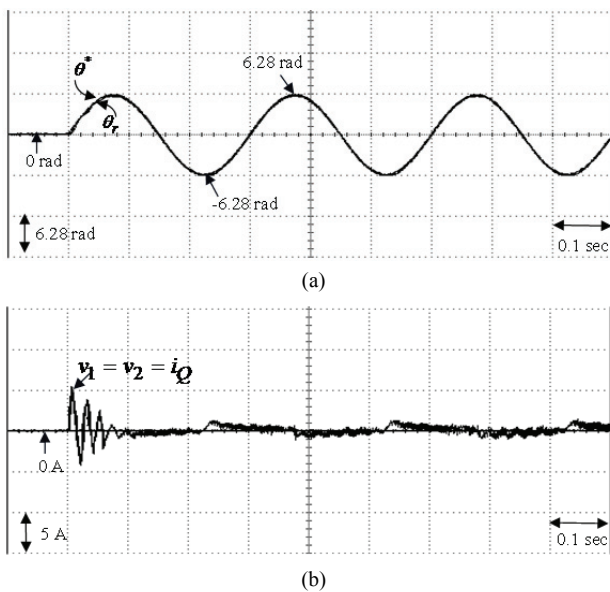

(a)

(b)

Fig. 20. Experimental results obtained with the proposed nonlinear backstepping control system using an adaptive law attributed to Case 4: (a) Position response of the rotor, (b) Response of the control effort, i.e., torque current i_Q.

Fig. 20, respectively. From these experimental results, better tracking responses of the position are obtained for controlling the SynRM drive system using the proposed nonlinear backstepping control system using an adaptive law due to the adaptive mechanism action. The position responses of the rotor under Case 3 and Case 4 are shown in Figs. 19(a) and 20(a), respectively. The associated control efforts, i.e., torque current i_Q, are shown in Figs. 19(b) and 20(b), respectively. Good tracking responses of the position can be obtained by

means of the proposed nonlinear backstepping control system using an adaptive law under the nominal case shown in Figs. 17(a) and 19(a), respectively. Moreover, the good tracking responses of the position shown in Figs. 18(a) and 20(a) are evident under the bigger nonlinear disturbance.

The parameters of the proposed nonlinear backstepping control system using the reformed recurrent Hermite polynomial neural network with an adaptive law and an error estimated law are given as $k_1 = 2.2$, $k_2 = 1.7$, $k_3 = 2.3$, $\gamma = 0.1$ and $\tau = 0.5$ according to heuristic knowledge [11], [12], [14], [17], [19], which results in a periodic step command from 0 rad to 6.28 rad in the nominal case to achieve good transient and steady-state control performances.

Furthermore, to show the effectiveness of the control system with a small number of neurons, the reformed recurrent Hermite polynomial neural network has 2, 4 and 1 neurons in the input layer, the hidden layer and the output layer, respectively. The parameter adjustment process remains continually active for the duration of the experiment. Parameter initialization of the reformed recurrent Hermite polynomial neural network in [28] is adopted to initialize the parameters. The parameter adjustment process remains continually active for the duration of the experiment. Experimental results of the proposed nonlinear backstepping control system using the reformed recurrent Hermite polynomial neural network with an adaptive law and an error estimated law for controlling the SynRM drive systems attributed to Case 1 and Case 2 are shown in Figs. 21 and 22, respectively.

Position responses of the rotor under Case 1 and Case 2 are shown in Figs. 21(a) and 22(a), respectively. In addition, the associated control efforts, i.e., torque current i_Q, are shown in Figs. 23(b) and 24(b), respectively. Experimental results of the proposed nonlinear backstepping control system using the reformed recurrent Hermite polynomial neural network with an adaptive law and an error estimated law for controlling the SynRM drive systems attributed to Case 3 and Case 4 are shown in Fig. 23 and Fig. 24, respectively. Position responses of the rotor under Case 3 and Case 4 are shown in Figs. 23(a) and 24(a), respectively. The associated control efforts, i.e., torque current i_Q, are shown in Figs. 23(b) and 24(b), respectively. The best tracking responses of the position can be obtained by means of the proposed nonlinear backstepping control system using the reformed recurrent Hermite polynomial neural network with an adaptive law and an error estimated law under Case 1 and Case 3 as shown in Figs. 21(a) and 23(a), respectively. Moreover, the excellent tracking responses of the position shown in Figs. 22(a) and 24(a) are very conspicuous under a bigger nonlinear disturbance. From these experimental results, better tracking responses of the position are obtained by using the proposed nonlinear backstepping control system using the reformed
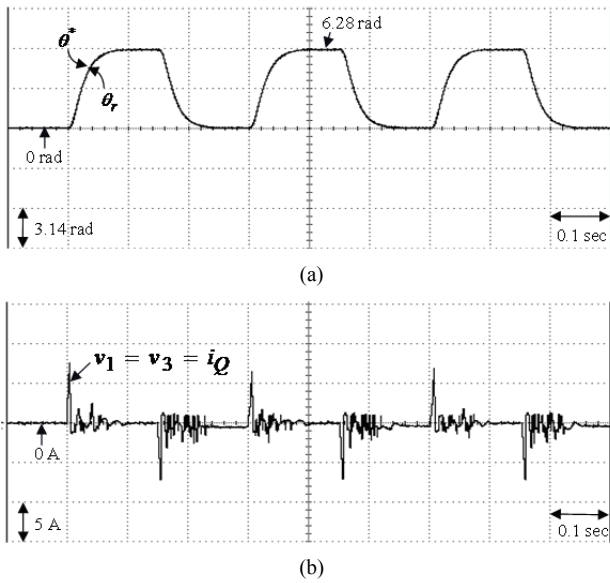
(a)

(b)

Fig. 21. Experimental results obtained with the proposed nonlinear backstepping control system using the reformed recurrent Hermite polynomial neural network with an adaptive law and an error estimated law attributed to Case 1: (a) Position response of the rotor, (b) Response of the control effort, i.e., torque current i_Q.

(a)

(b)

Fig. 23. Experimental results obtained with the proposed nonlinear backstepping control system using the reformed recurrent Hermite polynomial neural network with an adaptive law and an error estimated law attributed to Case 3: (a) Position response of the rotor, (b) Response of the control effort, i.e., torque current i_Q.

(a)

(b)

Fig. 22. Experimental results obtained with the proposed nonlinear backstepping control system using the reformed recurrent Hermite polynomial neural network with an adaptive law and an error estimated law attributed by Case 2: (a) Position response of the rotor, (b) Response of the control effort, i.e., torque current i_Q.
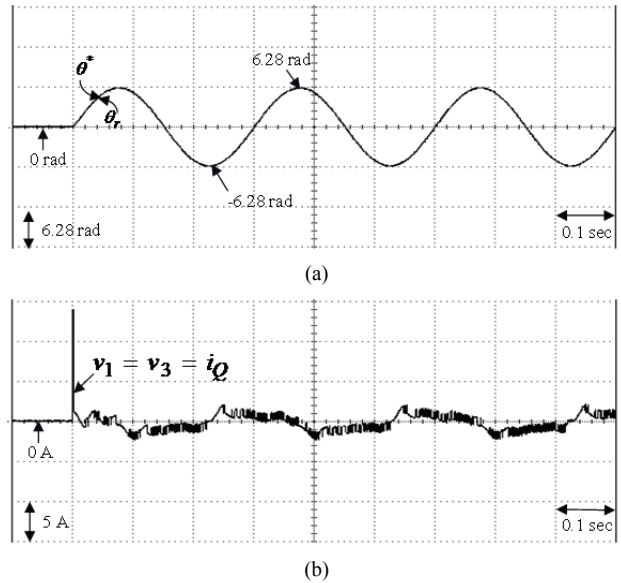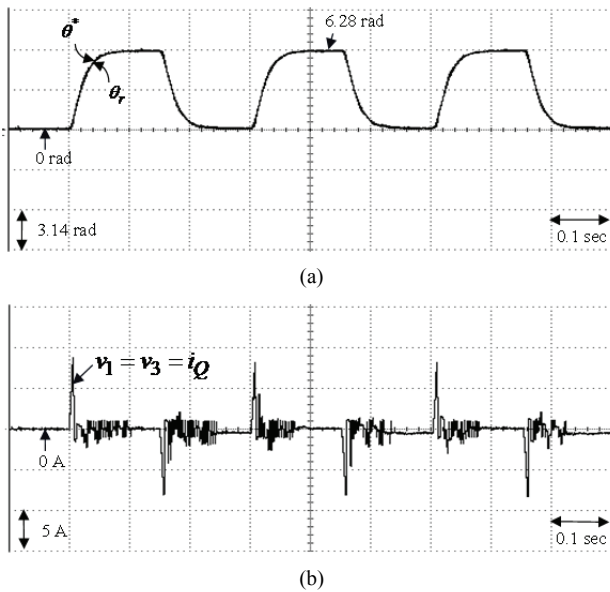

(a)

(b)
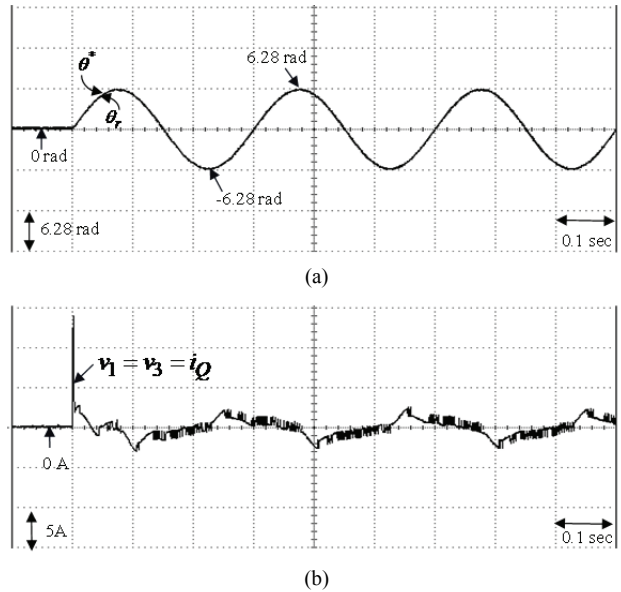
Fig. 24. Experimental results obtained with the proposed nonlinear backstepping control system using the reformed recurrent Hermite polynomial neural network with an adaptive law and an error estimated law attributed to Case 4: (a) Position response of the rotor, (b) Response of the control effort, i.e., torque current i_Q.

recurrent Hermite polynomial neural network with an adaptive law and an error estimated law for controlling SynRM drive systems.

Finally, experimental results of the measured rotor position response caused by Case 5 are shown in Fig. 25. Experimental

results of the measured rotor position responses by means of the conventional PI controller, the proposed nonlinear backstepping control system using an upper bound with a switching function, the proposed nonlinear backstepping control system using an adaptive law, and the proposed

Fig. 25. Experimental results of the measured rotor position response under Case 5 by means of: (a) The conventional PI controller, (b) The proposed nonlinear backstepping control system using an upper bound with a switching function, (c) The proposed nonlinear backstepping control system using an ada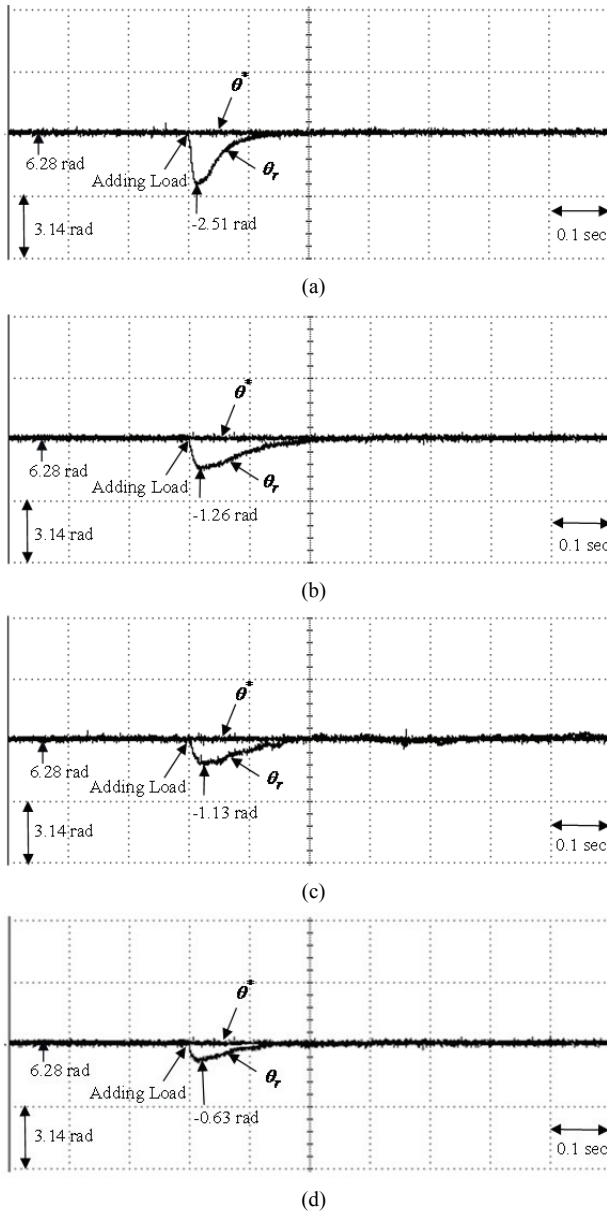ptive law, (d) The proposed nonlinear backstepping control system using the reformed recurrent Hermite polynomial neural network with an adaptive law and an error estimated law.

nonlinear backstepping control system using the reformed recurrent Hermite polynomial neural network with an adaptive law and an error estimated law under Case 5 are shown in Figs. 25(a), 25(b), 25(c) and 25(d), respectively. From these experimental results, the transient response of the proposed nonlinear backstepping control system using the reformed recurrent Hermite polynomial neural network with an adaptive law and an error estimated law is better than those of the conventional PI controller, the proposed nonlinear

TABLE I
PERFORMANCE COMPARISONS OF FOUR CONTROL SYSTEMS
WITH RESPECT TO FIVE TEST CASES

Per-formance	Conventional PI controller				
	Case 1	Case 2	Case 3	Case 4	Case 5
ME of d_1	0.64 rad	1.28 rad	0.72 rad	1.26 rad	2.51 rad
RMSE of d_1	0.45 rad	0.91 rad	0.53 rad	0.89 rad	1.77 rad
Per-formance	Control system A				
	Case 1	Case 2	Case 3	Case 4	Case 5
ME of d_1	0.62 rad	0.65 rad	0.61 rad	0.64 rad	1.26 rad
RMS error of d_1	0.44 rad	0.46 rad	0.42 rad	0.45 rad	0.89 rad
Per-formance	Control system B				
	Case 1	Case 2	Case 3	Case 4	Case 5
ME of d_1	0.60 rad	0.63 rad	0.58 rad	0.62 rad	1.13 rad
RMSE of d_1	0.42 rad	0.45 rad	0.41 rad	0.44 rad	0.81 rad
Per-formance	Control system C				
	Case 1	Case 2	Case 3	Case 4	Case 5
ME of d_1	0.54 rad	0.58 rad	0.52 rad	0.56 rad	0.63 rad
RMSE of d_1	0.36 rad	0.41 rad	0.37 rad	0.40 rad	0.45 rad

backstepping control system using an upper bound with a switching function and the proposed nonlinear backstepping control system using an adaptive law under load regulation.

However, the robust control performance of the proposed nonlinear backstepping control system using the reformed recurrent Hermite polynomial neural network with an adaptive law and an error estimated law was outstanding for the tracking of periodic steps and sinusoidal commands under the occurrence of parameter disturbances and load regulation due in large part to the on-line adaptive adjustment of the reformed recurrent Hermite polynomial neural network.

Additionally, a comparison of the control performances of the conventional PI controller, the proposed nonlinear backstepping control system using an upper bound with a switching function, the proposed nonlinear backstepping control system using an adaptive law, and the proposed nonlinear backstepping control system using the reformed recurrent Hermite polynomial neural network with an adaptive law and an error estimated law is summarized in Table I with respect to the experimental results of five test cases.

The maximum errors (ME) of d_1 using the conventional PI controller with: control system A - the proposed nonlinear backstepping control system using an upper bound with a switching function; control system B - the proposed nonlinear backstepping control system using an adaptive law; and control system C: the proposed nonlinear backstepping control system using the reformed recurrent Hermite polynomial neural network with an adaptive law and an error estimated law attributed to Case 1 are 0.64 rad, 0.62 rad, 0.60 rad and 0.54 rad, respectively. In addition, the RMS errors

TABLE II
CHARACTERISTIC PERFORMANCE COMPARISONS
OF FOUR CONTROL SYSTEMS

Characteristic performance	Convention al PI controller	Control system A	Control system B	Control system C
Chattering of control effort	Small	Large	Middle	Small
Dynamic response	Slow	Fast	Faster	Fastest
Load regulation ability	Poor	Good	Better	Best
Convergence speed	None	Fast	Faster	Fastest
Position tracking error	Large	Middle	Middle	Small
Parameter disturbance rejection	Poor	Good	Better	Best
Learning rate	None	None	None	Vary (Optimal learning rate)

(RMSE) of d_1 are 0.45 rad, 0.44 rad, 0.42 rad and 0.36 rad, respectively. The ME of d_1 by using the conventional PI controller with: control system A, control system B and control system C attributed to Case 2 are 1.28 rad, 0.65 rad, 0.63 rad and 0.58 rad, respectively. In addition, the RMSE of d_1 are 0.91 rad, 0.46 rad, 0.45 rad and 0.41 rad, respectively. The ME of d_1 by using the conventional PI controller with: control system A, control system B and control system C attributed to Case 3 are 0.72 rad, 0.61 rad, 0.58 rad and 0.52 rad, respectively. In addition, the RMSE of d_1 are 0.53 rad, 0.42 rad, 0.41 rad and 0.37 rad, respectively. The ME of d_1 by using the conventional PI controller with: control system A, control system B and control system C attributed to Case 4 are 1.26 rad, 0.64 rad, 0.62 rad and 0.56 rad, respectively. In addition, the RMSE of d_1 are 0.89 rad, 0.45 rad, 0.44 rad and 0.40 rad, respectively. The ME of d_1 by using the conventional PI controller with: control system A, control system B and control system C attributed to Case 5 are 2.51 rad, 1.26 rad, 1.13 rad and 0.63 rad, respectively. In addition, the RMSE of d_1 are 1.77 rad, 0.89 rad, 0.81 rad and 0.45 rad, respectively. As shown in the table, control system C results in a smaller tracking error in comparison with using the conventional PI controller, control system A and control system B. According to the tabulated measurements, control system 4 yields superior control performance.

Furthermore, characteristic performances comparisons of the conventional PI Controller, control systems A, control system B and control system C are summarized in Table II with respect to experimental results. As shown in the table, the various performances of control system C are superior to those of the conventional PI Controller, control systems A

and control system B in terms of characteristic performances such as chattering of the control effort, dynamic response, load regulation capability, convergence speed, position tracking error and parameter disturbance rejection.

V. CONCLUSIONS

A nonlinear backstepping control system using the reformed recurrent Hermite polynomial neural network with an adaptive law and an error estimated law is proposed to control a SynRM drive system for the position tracking of periodic reference inputs and load regulation.

The main contributions of this paper are as follows. 1) The field-oriented mechanism has been successfully applied to the control of a SynRM drive system. 2) The controller design of the nonlinear backstepping control system using an upper bound with a switching function has been successfully derived according to the Lyapunov function under a lumped uncertainty disturbance. 3) The controller design of the nonlinear backstepping control system using an adaptive law to estimate the lumped uncertainty has been successfully derived according to the Lyapunov function for reducing the chattering affect. 4) The control design of the nonlinear backstepping control system using the reformed recurrent Hermite polynomial neural network with an adaptive law and an error estimated law to estimate lumped uncertainty and to compensate estimated errors has been successfully derived according to the Lyapunov function for diminishing the lumped uncertainty effect. 5) The reformed recurrent Hermite polynomial neural network with two varied learning rates has been successfully derived according to the increment type Lyapunov function to speed-up the parameter convergence.

Furthermore, as indicated by the experimental results and Table I, the proposed nonlinear backstepping control system using the reformed recurrent Hermite polynomial neural network with an adaptive law and an error estimated law has a smaller tracking error and better disturbance rejection in comparison with the conventional PI controller, the proposed nonlinear backstepping control system using an upper bound with a switching function and the proposed nonlinear backstepping control system using an adaptive law.

Finally, comparisons of the various control performances shown in Table II for the four control systems verified that the proposed nonlinear backstepping control system using the reformed recurrent Hermite polynomial neural network with an adaptive law and an error estimated law for controlling a SynRM drive system is superior to those of the conventional PI controller, the proposed nonlinear backstepping control system using an upper bound with a switching function and the proposed nonlinear backstepping control system using an adaptive law with respect to the chattering of the control effort, dynamic response, capability of load regulation, position tracking error and parameter disturbance rejection.

REFERENCES

[1] V. Dmitrievskii, V. Prakht, V. Kazakbaev, A. Pozdeev, and S. Oshurbekov, "Development of a high efficient electric drive with synchronous reluctance motor," in *Intl. Conf. on Electrical Machines and Systems* (ICEMS), pp. 876-881, 2015.

[2] V. Kazakbaev, V. Prakht, V. Dmitrievskii, and I. Sokolov, "The feasibility study of the application of a synchronous reluctance motor in a pump drive," in *Intl. Conf. on Power Drives Systems* (*ICPDS*), 2016.

[3] K. C. Kim, J. S. Ahn, S. H. Won, J. P. Hong, and J. Lee , "A study on the optimal design of SynRM for the high torque and power factor," *IEEE Trans. Magn.*, Vol. 43, No. 6, pp. 2543-2545, Jun. 2007.

[4] Y. H. Kim and J. H. Lee, "Optimum design criteria of an ALA-SynRM for the maximum torque density and power factor improvement," *Int. J. Applied Electromagn. Mech.,* Vol. 53, No. S2, pp. S279-S288, 2017.

[5] W. Chai, W. Zhao, and B. Kwon, "Optimal design of wound field synchronous reluctance machines to improve torque by increasing the saliency ratio," *IEEE Trans. Magn.*, Vol. 53, No. 11, Nov. 2017.

[6] T. Matsuo, A. E. Antably, and T. A. Lipo, "A new control strategy for optimum-efficiency operation of a synchronous reluctance Motor," *IEEE Trans. Ind. Electron.*, Vol. 33, No. 5, pp. 1146-1153, Sep./Oct. 1997.

[7] E. M. Rashad, T. S. Radwan, and M. A. Rahman, "A maximum torque per ampere vector control strategy for synchronous reluctance motors considering saturation and iron losses," *in IEEE Industry Applications Annual Meeting*, pp. 2411-2417, 2004.

[8] C. H. Lin, "Adaptive recurrent fuzzy neural network control for synchronous reluctance motor servo drive," *IEE Proc. Electric Power Appl.,* Vol. 151, No. 6, pp. 712-724, Nov. 2004.

[9] M. Y. Wei and T. H. Liu, "Design and implementation of an online tuning adaptive controller for synchronous reluctance motor drives," *IEEE Trans. Ind. Electron.*, Vol. 60, No. 9, pp. 3644-3657, Sep. 2013.

[10] H. K. Chiang and C.T. Chu, "Reference model with an adaptive Hermite fuzzy neural network controller for tracking a synchronous reluctance motor," *Electric Power Compon. Syst.*, Vol. 43, No. 7, pp. 770-780, Apr. 2015.

[11] I. Kanellakopoulos, P. V. Kokotovic, and A. S. Morse, "Systematic design of adaptive controller for feedback linearizable system," *IEEE Trans. Autom. Contr.*, Vol. 36, No. 11, pp. 1241-1253, Nov. 1991.

[12] Bartolini, A. Ferrara, L. Giacomini and E. Usai, "Peoperties of a combined adaptive/second-order sliding mode control algorithm for some classes of uncertain nonlinear systems," *IEEE Trans. Autom. Contr.*, Vol. 45, No. 7, pp. 1334-1341, Jul. 2000.

[13] S. I. Amer and M. M. Salem, "A comparison of different intelligent control techniques for a PM dc motor," *J. Power Electron.*, Vol. 5, No. 1, pp. 1-10, Jan. 2005.

[14] C. H. Lin, "A backstepping control of LSM drive systems using adaptive modified recurrent Laguerre OPNNUO," *J. Power Electron.*, Vol. 16, No. 2, pp. 598-609, Mar. 2016.

[15] A. F. Payam, M. N. Hashemnia, and J. Faiz, "Robust DTC control of doubly-fed induction machines based on input-output feedback linearization using recurrent neural networks," *J. Power Electron.*, Vol. 11, No. 5, pp. 719-725, Sep. 2011.

[16] C. H. Lin "Hybrid recurrent wavelet neural network control of PMSM servo-drive system for electric scooter," *Int. J. Contr., Autom. Syst.*, Vol. 12, No. 1, pp. 177-187, Feb. 2014.

[17] C. H. Lin, "A PMSM driven electric scooter system with V-belt continuously variable transmission using novel hybrid modified recurrent Legendre neural network control," *J. Power Electron.*, Vol. 14, No. 5, pp.1008-1027, Sep. 2014.

[18] C. H. Lin, "Novel adaptive recurrent Legendre neural network control for PMSM servo-drive electric scooter," *J. Dynamic Syst., Meas., Contr.- Trans. ASME*, Vol. 137, 011010-1, Jan. 2015.

[19] C. H. Lin, "Nonlinear backstepping control design of LSM drive system using adaptive modified recurrent Laguerre othognal polynomial network," *Int. J. Contr., Autom. Syst.*, Vol. 15, No. 2, pp. 905-917, Apr. 2017.

[20] L. Ma and K. Khorasani, "Constructive feedforward neural networks using Hermite polynomial activation functions," *IEEE Trans. Neural Netw.,* Vol. 16, No. 4, pp. 821-833, Jul. 2005.

[21] L. Ma and K. Khorasani, "Adaptive constructive neural networks using Hermite polynomials for image compression," in *Intl. Symp. on Neural Networks*, pp 713-722, 2005.

[22] G. G. Rigatos and S. G. Tzafestas, "Feed-forward neural networks using Hermite polynomial activation functions," *4th Helenic Conference on Advances in Artificial Intelligence, SETN 2006,* pp. 323-333, 2006.

[23] S. M. Siniscalchi, J. Li, and C. H. Lee, "Hermitian polynomial for speaker adaptation of connectionist speech recognition systems," *IEEE Trans. Audio, Speech, Language Process.*, Vol. 21, No. 10, pp. 2152-2161, Oct. 2013.

[24] J. J. E. Slotine and W. Li, *Applied Nonlinear Control,* Englewood Cliffs, NJ: Prentice-Hall, 1991.

[25] J. Astrom and B. Wittenmark, *Adaptive Control,* New York: Addison-Wesley, 1995.

[26] C. C. Ku and K. Y. Lee, "Diagonal recurrent neural networks for dynamic system control," *IEEE Trans. Neural Netw.*, Vol. 6, No. 1, pp.144-156, Jan. 1995.

[27] C. H. Lin, "Recurrent modified Elman neural network control of PM synchronous generator system using wind turbine emulator of PM synchronous servo motor drive," *Int. J. Electr. Power Energy Syst.,* Vol. 52, pp. 143-160, Nov. 2013.

[28] F. L. Lewis, J. Campos, and R. Selmic, *Neuro-Fuzzy Control of Industrial Systems with Actuator Nonlinearities.* SIAM Frontiers in Applied Mathematics, 2002.

[29] K. J. Astrom and T. Hagglund, *PID Controller: Theory, Design, and Tuning,* North Carolina: Instrument Society of America, Research Triangle Park, 1995.

[30] T. Hagglund and K. J. Astrom, "Revisiting the Ziegler-Nichols tuning rules for PI control," *Asian J. Contr.*, Vol. 4, No. 4, pp. 364-380, Dec. 2002.

[31] T. Hagglund and K. J. Astrom, "Revisiting the Ziegler-Nichols tuning rules for PI control-part II: The frequency response method," *Asian J. Contr.*, Vol. 6, No. 4, pp. 469-482, Dec. 2004.

[32] F. J. Lin and C. H. Lin, "On-line gain-tuning IP controller using RFNN," *IEEE Trans. Aerosp. Electron. Syst.*, Vol. 37, No. 2, pp. 655-670, Apr. 2001.

Jung-Chu Ting was born in Pingtung, Taiwan. He received his M.S. degree from Dayeh University, Changhua, Taiwan, in 2004. He became a Ph.D. candidate at the National Changhua University of Education, Changhua, Taiwan, in 2017. His current research interests include power electronics, applications of control theory, and motor controls.

Der-Fa Chen was born in Taipei, Taiwan. He received his M.S. degree from the National Chiao Tung University, Hsinchu, Taiwan, in 1988; and his Ph.D. degree from the National Taiwan University of Science and Technology, Taipei, Taiwan, in 2000. From February 2003 to July 2006, he was an Associate Professor in the Department of Industrial Education and Technology, National Changhua University of Education, Changhua, Taiwan, where he has been working as a Professor since August 2006. His current research interests include power electronics, applications of control theory, and motor controls.